JOURNAL OF CATALYSIS **163,** 418–428 (1996)
ARTICLE NO. 0343

Promoter Effect of Cesium on C–C Bond Formation during Alcohol Synthesis from CO/H_2 over $Cu/ZnO/Cr_2O_3$ Catalysts

J. M. Campos-Martín,* J. L. G. Fierro,*,[1] A. Guerrero-Ruiz,† R. G. Herman,‡ and K. Klier‡

Instituto de Catálisis y Petroleoquímica, C.S.I.C., Campus UAM, Cantoblanco, 28049 Madrid, Spain; †Departamento de Química Inorgánica, U.N.E.D., Senda del Rey s/n, Ciudad Universitaria, 28040 Madrid, Spain; ‡Department of Chemistry and Zettlemoyer Center for Surface Studies, Lehigh University, Bethlehem, Pennsylvania 18015

Received January 31, 1996; revised May 28, 1996; accepted June 11, 1996

The effect of calcination temperature and Cs-promotion on the ternary Cu–Zn–Cr oxide catalyst has been investigated in connection with both structural and catalytic properties in the high pressure CO hydrogenation. As revealed by TPR and XPS, the reduction of copper is inhibited by incorporation of Cs promoter. Under typical reaction conditions, detectable copper phases are reduced to metallic copper. The crystal size of copper particles tends to increase with increasing reduction temperature and simultaneously Cs is segregated to the catalyst surface. Activity results in CO hydrogenation, with and without cofeeding methanol, ethanol, or 1-propanol, showed that methanol or $C_{2+}OH$ yield increased upon Cs-doping of the catalysts. By feeding a given C_nOH alcohol, the $C_{n+}OH$ yield was enhanced, with the most difficult chain growth being for the reaction $CH_3OH \rightarrow CH_3CH_2OH$. While a large surface area of the catalysts, with ill-defined crystalline phases, is the key parameter for an enhancement in the productivity and a low increase in the selectivity to higher alcohols, cesium incorporation leads to substantial improvement in $C_{2+}OH$ selectivity.

INTRODUCTION

An efficient process for the synthesis of higher alcohols from synthesis gas (hydrogen and carbon monoxide) is of evident interest, in the first place because alcohols (especially methanol and ethanol) are important in the synthesis of several chemical products and in the second place alcohols can be used as additives to gasoline or as liquid fuel of high octane number. Mixed alcohols are preferred to methanol as a gasoline octane enhancer because of the cosolvent effect of the higher alcohols. As straight liquid fuels, the heat of combustion of alcohols on unit mass or unit volume basis increases with molecular weight. Moreover, the addition of alcohols to gasoline not only increases the RON (research octane number), but it also reduces the level of CO, NO_x, and unburned hydrocarbons in the exhaust.

On the other hand, the new more restrictive regulations for the reformulate gasolines in USA and EU help to increase the incorporation of oxygenates into liquids fuels, i.e., ethers, such as MTBE (methyl tert-buthyl ether), and alcohols. The European regulation 85/536/ECC (1) specifies that all country members of EU have to establish the minimum level of oxygenates in gasolines up to the limits showed in the Table 1.

Formation of higher alcohol on methanol synthesis catalysts is enhanced by doping with alkali metal ions, as has been shown to occur both over the high-pressure (20.3–25.5 MPa) and high-temperature (673–723 K) zinc chromite catalysts (2, 3) and the low-pressure (2–10 MPa) and low-temperature (500–600 K) copper-based catalysts (4–7). One of the earliest studies was conducted by Morgan *et al.* (8, 9), who found cesium as an effective promoter of higher oxygenate synthesis over a Cr_2O_3/MnO catalyst. Several authors (10–14) reported that over the copper-based catalysts, heavy alkali ions are also effective promoters for higher oxygenate synthesis. However, the effect of alkali doping on the synthesis of methanol has been reported to involve mainly a fall in catalytic activity and a decrease of the selectivity to methanol (4, 8, 15). Over transition metal catalysts such as palladium supported on silica (16), alkali doping inhibited methanol formation, whereas over copper-based methanol synthesis catalysts, the patent literature (17) specifies that the absence of alkali from catalyst composition for the selective synthesis of methanol is required. However, it has been demonstrated that a heavy alkali, particularly cesium, also promotes methanol synthesis when used at optimum surface concentrations (19).

Numerous reaction mechanisms have been proposed for methanol synthesis, and the development of mechanistic concepts has been summarized and discussed elsewhere (12–14, 20–23). The existence of formate, methoxy, formyl, and aldehydic intermediates on the surface of the Cu/ZnO-based catalysts have been firmly established by using several techniques such as "*in situ*" infrared spectroscopy (24, 25), chemical trapping (26–28), isotope labeling (12–14, 29), and temperature-programmed desorption (30–33). Formyl or aldehydic intermediates are significant for higher alcohols synthesis, in view easily of mechanistic

[1] To whom the correspondence should be addressed.

0021-9517/96 $18.00

TABLE 1

Oxygenate Levels in Reformulated Gasolines

Additive	Limit	
	Accepted (vol%)	For required labelling (vol%)
MTBE	10	15
Methanol	3	3
Ethanol	5	5
Isoproponol	5	10
t-Butanol	7	7
Isobutanol	7	10
Total oxygen content (wt%)	2.5	3.7

proposals put forward by Morgan *et al*. (8, 9), which suggest that the synthesis occurs via aldol coupling of the C_1 intermediate with other aldehydic intermediates, followed by partial dehydration and hydrogenation. A similar reaction mechanism has been invoked by other authors (10–14) and the promotional effect of heavy alkali metal ions, such as cesium, for the synthesis of higher alcohols was explained using it.

The synthesis of ethanol has been proposed to occur by several paths. These can be divided into three principal categories: direct synthesis from CO/H_2,

$$2CO + 4\,H_2 \rightarrow C_2H_5OH + H_2O, \qquad [1]$$

homologation of methanol by CO/H_2,

$$CH_3OH + CO + 2H_2 \rightarrow C_2H_5OH + H_2O, \qquad [2]$$

and coupling of two methanol molecules,

$$2CH_3OH \rightarrow C_2H_5OH + H_2O. \qquad [3]$$

Reaction [1] has been proposed for the synthesis of ethanol over supported Rh catalysts (34, 35), while reaction [2] has been employed to describe alcohol formation via Fischer–Tropsch-type synthesis catalysts (3, 36). The synthesis of ethanol over modified methanol synthesis catalysts has been proposed (3, 12–14) to occur by reaction [3] or its modification [4], and higher alcohols would be formed by analogous surface-catalyzed coupling reactions,

$$2CH_3OH \xrightarrow{-2H_2} [H_2C(CO)CHO] \xrightarrow{+2H_2} C_2H_5OH + H_2O. \qquad [4]$$

The intention in undertaking this work was to concentrate attention upon the promotional effect of cesium in Cu–Zn–Cr catalysts. In order to understand the structure and properties of these catalysts, several characterization techniques were applied, such as X-ray powder diffraction, temperature programmed reduction, X-ray photoelectron spectroscopy, temperature programmed surface reaction, and catalytic activity measurements.

EXPERIMENTAL

Catalyst Preparation

The catalysts used in this study were prepared following the coprecipitation method (37, 38). In this case, to an aqueous solution of the copper, zinc, and chromium nitrates of appropriate concentration, a 0.5 *M* ammonium bicarbonate (all Merck reagent grade) solution was gradually added with stirring until a final pH approximately 7.5 was reached. After filtration, the precipitate was repeatedly washed to remove the major fraction of adsorbed NH_4^+, CO_3^{2-}, and NO_3^- ions and then dried at 393 K. The dry precursors were then calcined in air either at 673 K or at 553 K (samples denoted A and B, respectively) for 24 h. Portions of the catalyst were doped with cesium, wherein 25 ml of the appropriate solution of cesium nitrate was added to obtain a cesium concentration in the catalyst of 8 wt% and then the solvent was evaporated to dryness. The final composition was determined by atomic absorption spectrometry. The calcined catalysts were subsequently pelleted, ground, and sieved to particle sizes of 0.59–0.42 mm. For the sake of simplicity, the catalysts will be referred to hereafter as A (or B), the catalyst calcined at 673 K (or 553 K) and as CsA (CsB), the catalyst A (or B) doped with cesium.

Instrumental Techniques

X-Ray powder diffraction (XRD) patterns were recorded from both calcined and used catalysts using an APD 1700 automated powder diffractometer system 1, using nickel-filtered Cu$K\alpha$ radiation ($\lambda = 0.l538$ nm), under constant instrumental parameters. For each sample, Bragg's angles between 5° and 75° were scanned at a rate of 2°/min. Specific surface areas of the catalysts were calculated by applying the BET method to the N_2 adsorption isotherms, measured at liquid nitrogen temperature on a Micromeritics ASAP 2000 instrument and taking a value of 0.162 nm^2 for the cross section of the adsorbed nitrogen molecule.

TPR experiments were carried out in a Cahn 2000 microbalance at a sensitivity of 10 μg. The samples (5–10 mg) were heated in a flow (60 ml/min) of 5% volume of air in helium (99.999% vol) up to 473 K in order to remove adsorbed water and other gaseous contaminants. Following cooling to room temperature in the same flow of helium, the gas flow was switched to a reducing mixture (60 ml/min) of 5% volume hydrogen (99.995% vol) in helium, and the sample was again heated at a rate of 4 K/min up to 673 K while continuously recording the weight changes. The microbalance was interfaced to a microcomputer that allowed accumulation and processing of weight change–temperature curves.

X-ray photoelectron spectra were acquired with a Fisons ESCALAB 200R spectrometer equipped with a hemispherical electron analyzer and a Mg$K\alpha$ 120 W X-ray source. The powder samples were pressed into

small aluminum cylinders and then mounted on a sample rod placed in a pretreatment chamber and heated under vacuum at 373 K for 1 h prior to being moved into the analysis chamber. After analysis, the same catalyst sample was moved to the pretreatment chamber and reduced *in situ* by hydrogen at 473, 523, and 673 K. The pressure in the ion-pumped analysis chamber was below 3×10^{-9} Torr (1 Torr = 133.33 Pa) during data acquisition. The intensities were estimated by calculating the integral of each peak after smoothing and subtraction of the "S-shaped" background and fitting the experimental curve to a mix of Lorentzian and Gaussian lines of variable proportion. All binding energies (BE) were referenced to the adventitious C 1s line at 284.9 eV. This reference gave BE values within an accuracy of ±0.2 eV.

Temperature Programmed Surface Reaction (TPSR)

TPSR experiments were performed on aliquots of catalysts (50 mg) placed in a glass reactor assembled to a vacuum line and gas-handling system. The samples were reduced in hydrogen at 473 K for 2 h and then outgassed at 10^{-6} Pa for 1 h at 673 K. Subsequently, they were cooled to room temperature and exposed to a methanol pulse (4.1 Pa) for 15 min. The methanol used was 99.9% pure (Riedel de–Häen), and it was taken through several freeze-pump-thaw cycles before use. Once the gas phase was removed, the samples were heated to 673 K using a constant heating rate of 5 K/min. A Balzers QMG 421C quadrupolar mass spectrometer, connected in-line with the reactor was used for analysis of the desorption products. The products were identified by comparing their cracking pattern in the mass spectrometer with the m/e values in the following list: H_2 (2), CH_4 (15, 16), H_2O (18), CO (28), CH_2O (28, 29, 30), CH_3OH (29, 31, 32), CO_2 (28, 44), $(CH_3)_2O$ (29, 45, 46), C_2H_4 and C_2H_6 (26, 27, 28), C_2H_4O (29, 43, 44), C_2H_5OH (29, 31, 45, 46), and $(C_2H_5)_2O$ (29, 31, 45, 59, 74).

Catalytic Activity Measurements

The activity tests were carried out using a semiautomatic high pressure fixed-bed catalytic reactor. The reactor was a copper lined stainless steel tube. The catalyst (2.45 g) was held in place in the middle of the reactor by Pyrex beads, with the top of the reactor filled with Pyrex beads serving as a preheater. A K-type thermocouple placed in the catalyst bed was used to measure the reaction temperature. The composition of the feed stream, CO (69% vol) and H_2 (31% vol), was adjusted by electronic mass flow controllers (Linde/Union Carbide) to yield a spatial velocity of 3200 $l(SPT)/g_{cat} \cdot h$. The reaction was conducted to 7.6 MPa overall pressure and reaction temperatures of 548 and 583 K (only the latter temperature for catalysts calcined at 673 K). The reaction leading sequence started with feeding the CO/H_2 mixture, and after 6 h on-stream alcohols were sequentially injected in the following order: methanol, ethanol, and 1-propanol. The alcohols were introduced into the synthesis gas at the inlet of the reactor using a high-pressure continuous-feed Model 302 GILSON pump at the rate of 0.4 mmol/min. All experimental data were obtained under steady-state conditions that were usually maintained for 5–10 h before changing the reaction conditions to obtain another set of data. The effluents of the reactor were analyzed by GC, using an on-line automated sampling valve. To avoid condensation of the reaction products, the outlet of the reactor was heated to 423 K. A Hewlett–Packard 5730A gas chromatograph, coupled with a Hewlett–Packard Model 3393, Series II integrator, equipped with a Porapack Q column was used for product separation. The analysis of the products, CO, CO_2, C_1–C_6 hydrocarbons and C_1–C_4 alcohols, was carried out with a thermal conductivity detector (TCD).

RESULTS AND DISCUSSION

Surface Areas

Table 2 compiles the chemical composition, crystalline phases detected by XRD and BET areas of different catalysts. The BET areas indicate clearly that an increase in calcination temperature from 553 to 673 K causes the surface area to decrease dramatically by one order of magnitude. In addition, incorporation of the cesium promoter did not seem to alter to a significant extent the BET area of the base catalyst.

X-Ray Diffraction

The crystalline phases present in both fresh and used catalysts were determined by X-ray powder diffraction. The

TABLE 2

Chemical Composition, BET Specific Surface Areas, and Crystalline Phases Detected by XRD in the Catalysts

Catalyst	Chemical composition (%mol)				S_{BET} (m^2/g)	Crystalline phases detected by XRD	
	Cu	Zn	Cr	Cs		Calcined	Tested
A	41	54	5	—	5.9	CuO, ZnO, Cr_2O_3, $ZnCr_2O_4$	Cu, ZnO, Cr_2O_3, $ZnCr_2O_4$
CsA	40	52	5	3	6.0	CuO, ZnO, Cr_2O_3, $ZnCr_2O_4$, $CsNO_3$	Cu, ZnO, Cr_2O_3, $ZnCr_2O_4$
B	38	54	8	—	62.8	CuO, ZnO	Cu, ZnO
CsB	37	52	7	4	64.4	CuO, ZnO, $CsNO_3$	Cu, ZnO

XRD pattern of the calcined catalyst A exhibited the presence of the oxides of copper, zinc, and chromium and a $ZnCr_2O_4$ spinel, whereas the same catalyst after catalytic treating displayed the same phases, with the exception of copper oxide, which had been reduced to metallic copper (Table 2). The catalyst calcined at lower temperature (B) was somewhat different; i.e., it was poorly crystallized and only showed copper and zinc oxides, but in no case were diffraction lines of the $ZnCr_2O_4$ spinel detected. The XRD patterns of this catalyst after CO hydrogenation treating were characteristic of unreduced ZnO and metallic copper, wherein the corresponding diffraction peaks were less intense and broader than those of the used catalyst A. This observation suggests that copper particles in the used catalyst were smaller than in the samples calcined at 553 K, due very likely to a less intensive sinterization of the copper particles under the conditions of CO hydrogenation in the catalyst of large surface area. For the Cs-promoted catalysts (CsA, CsB), the XRD patterns are complicated by the appearance of phases other than those mentioned above. Lines that appeared to be associated to cesium nitrate were the new diffraction peaks observed in the pattern of calcined Cs-promoted catalysts. These peaks disappeared after CO hydrogenation, suggesting that cesium nitrate is decomposed into its oxide, which in turn was poorly crystallized, or was highly dispersed among the other catalyst component. As was seen via the XPS to be described the Cs component became carbonated, either by the CO feed or by the CO_2 reaction product. An additional observation was the appearance of broader and less intense diffraction lines of copper metal in Cs-promoted (CsA, CsB) catalyst that in the unpromoted catalysts (A, B).

Temperature-Programmed Reduction (TPR)

Figure 1 displays the TPR profiles of the catalysts. The arbitrary unit value of 100 corresponded to the limiting value expected for the weight loss due to reduction of the CuO component to Cu. The weight loss above 100 was due to decomposition of hydroxocarbonate residue. From an inspection of these profiles several clues related to catalyst reducibility can be obtained. In the catalyst with high specific area (B), copper oxide was reduced at lower temperatures than it was in the catalyst (A) calcined at higher temperatures, and having lower surface area. It is noted that the crystal size of CuO of calcined catalyst B, as measured by XRD line broadening on the most intense diffraction peaks of this phase, was substantially smaller than for the parent catalyst A. These results, which are in accordance with previous TPR studies of CuO (39), point to an easier reduction by hydrogen of the CuO crystals with smaller average sizes. The comparison of TPR profiles for the unpromoted catalysts (A and B) and for the Cs-promoted homologous (CsA and CsB) indicates clearly that the presence of cesium retards CuO reduction by about 50 K. The

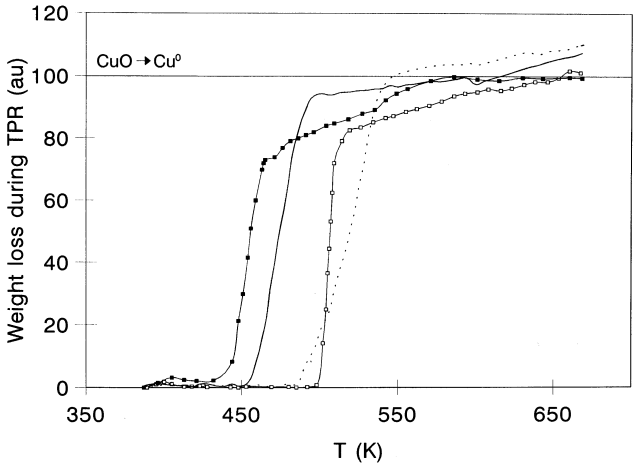

FIG. 1. Temperature programmed reduction profiles obtained in flowing 5% H_2/He of different catalysts: (———) A calcined at 673 K; (– – –) Cs-doped catalyst A; (■) B calcined at 553 K; (□) Cs-doped catalyst B.

retardation in the reduction of CuO might be associated to a closer interaction between the CuO phase and promoter which inhibited to some extent H_2 dissociation and therefore the nucleation centers of Cu^0. In addition, the onset temperature for the reduction of catalyst CsA was 480 K, the reduction was not completed until about 540 K. Although the TPR profile for the catalyst CsB was in the same temperature region, the window temperature for complete reduction of CuO in CsB was appreciably narrower, i.e. although some reduction continued to seem with both samples at higher temperature, the CuO reduction occurred between the temperatures 490 K and 500 K. The origin of a narrower temperature window for the reduction of CuO in catalyst CsB could be more physical than chemical. As the same hydrogen flow was maintained in all the experiments, mass transfer limitations at the gas–solid interface can be eliminated. However, diffusional effects of both hydrogen (reactant) and water (product) across a thick layer of metallic Cu on the outer surface of catalyst particles might well be operative in the catalyst with larger CuO particles (catalyst CsA) but not in its counterpart with smaller ones (catalyst CsB).

X-Ray Photoelectron Spectroscopy (XPS)

Photoelectron spectroscopy (XPS) was used for both qualitative and quantitative surface analysis of the catalysts. The binding energies (BE) of core electrons for catalysts A and B and their promoted counterparts CsA and CsB subjected to evaluation and various reductions pretreatments are compiled in Table 3. The binding energy of the Zn $2p_{3/2}$ peak was essentially constant for all the catalysts (ca 1021.7 eV), irrespective of the presence or absence of the Cs promoter and of the catalyst pretreatments, suggesting that Zn^{2+} ions were not reduced. Similarly, the BE of the

TABLE 3

Binding Energies (eV) of Core Electrons and the Auger Parameter (eV) of the Catalysts Subjected to Evacuation and to Varied *in Situ* Reduction Pretreatments

Catalyst	Treatment	Cr $2p_{3/2}$	Cs $3d_{5/2}$	Cu $2p_{3/2}$	Auger param.
A	Vacuum	577.9/575.5	—	933.4/935.2	—
	$T_r = 473$ K	576.0	—	933.1/932.1	—
	$T_r = 523$ K	575.9	—	932.1	—
	$T_r = 673$ K	576.3	—	932.3	—
CsA	Vacuum	578.2/575.7	726.7/724.5	935.0/933.4	—
	$T_r = 473$ K	575.6	724.7	934.0/932.4	—
	$T_r = 523$ K	575.6	724.5	933.8/932.2	—
	$T_r = 673$ K	575.5	724.8	932.8/931.8	—
B	Vacuum	578.9/576.4	—	934.2	1851.8
	$T_r = 473$ K	576.1	—	934.7/933.0	1851.5
	$T_r = 523$ K	576.4	—	932.6	1851.5
	$T_r = 673$ K	576.3	—	932.4	1851.4
CsB	Vacuum	579.2/576.8	726.7/724.6	934.0	1851.8
	$T_r = 473$ K	576.2	725.3	934.7/932.5	1851.5
	$T_r = 523$ K	576.0	725.5	932.4	1851.6
	$T_r = 673$ K	576.4	725.6	932.5	1851.5

Cs $3d_{5/2}$ peak in Cs-promoted catalyst was characteristic of cesium carbonate, which in turn appeared to be confirmed by the observation of a C 1s peak at BE ca 290 eV. The behavior of chromium was somewhat different. For all the reduced catalysts, the Cr $2p_{3/2}$ peak shows a single peak around 576 eV, typical of Cr^{3+} ions. However, the unreduced (both the unpromoted and Cs-promoted) catalysts displayed two peaks separated by 2.4–2.5 eV, the high BE peak which is dominant is associated to Cr^{6+} and the lower BE one to Cr^{3+}. The presence of both Cr^{6+} and Cr^{3+} species in these calcined Cu–Cr–Zn catalysts has been observed on fresh alumina-supported chromia catalysts, even for low chromia contents, but the Cr^{6+} ions disappeared in a reducing atmosphere, i.e., the oxidative dehydrogenation of propylene (40).

The Cu $2p_{3/2}$ line profiles of the catalyst were complex and changed dramatically upon reduction. This is illustrated in Figs. 2A and 2B for catalysts B and CsB, respectively. All outgassed catalysts showed the principal Cu $2p_{3/2}$ peak very broad, somewhat above 934 eV, and a satellite peak (Cu^{2+}_{sa}) at ca 943 eV. Upon reduction at 473 K, the Cu $2p_{3/2}$ peak is shifted to lower BE by 1.4–1.6 eV and simultaneously the satellite peak disappeared. A small high BE component was required in curve fitting of Cu $2p_{3/2}$ peak for catalysts A and B, and this component was in the same ratio as that at the lower BE for catalysts CsA and CsB (Fig. 2B, spectrum b). This later observation agrees with the shift of the onset temperature of reduction toward higher temperature in catalyst CsB. Finally, after reduction at 523 and 573 K only a narrow and symmetric peak at ca 932.4 eV is observed for all the catalysts.

Metallic copper and Cu^{2+} ions can easily be identified by XPS since the Cu $2p_{3/2}$ peak appears at a BE of 932.4 eV for Cu^0 and above 934.0 eV for Cu^{2+} ions. An additional means of identifying Cu^{2+} ions is the prominent satellite structure located at the high binding energy side. This satellite has been attributed to shake-up transitions by ligand → metal 3d charge transfer (41). This transfer cannot occur in Cu^+ compounds and Cu^0 because of their completely filled 3d shells. The identification of the reduced copper species, i.e., Cu^0 and/or Cu^+, becomes extremely difficult by XPS alone since the BE for Cu^0 and Cu^+ are almost the same, appearing at ca 1.6 eV below that of Cu^{2+} ions (42–44). This is only feasible through observation of the L_3VV X-ray induced Auger parameter of copper (see, e.g., 42, 44–47). The modified Auger parameter, α'_A, defined by Eq. (47) $\alpha'_A = h\nu + KE_{LMM} - KE$ Cu $2p_{3/2}$, is generally used for these analyses. KE_{LMM} and KE Cu $2p_{3/2}$ are the kinetic energies of the L_3VV X-ray induced Auger-emitted electrons and the Cu $2p_{3/2}$ photo-emitted electrons, respectively. The X-ray induced Auger parameters determined for catalyst B and its promoted CsB homologous are compiled in Table 3. Both outgassed catalysts were found to have the α'_A parameter at 1851.8 eV, which is characteristic of Cu^{2+} species (46). However, the catalysts reduced at 473, 523, and 573 K showed this parameter in the region of 1851.4–1851.6 eV, which is expected for Cu^0 (45–47). Since no other peak was observed in the reduced catalysts at energies as low as about 1849.7 eV, where Cu^+ ions are expected to appear (44–47), it can be inferred that the major reduced copper species is Cu^0 in both of the B and CsB reduced catalysts, although a minor proportion of Cu^+ cannot be completely ruled out.

Temperature-Programmed Surface Reaction (TPSR)

TPSR profiles obtained after adsorption of methanol on CuO, ZnO, and the multicomponent catalysts are displayed in Figs. 3–8. Every catalyst showed a desorption peak of methanol at low temperature ($T < 450$ K), which was accompanied by the additional two, corresponding to formaldehyde and hydrogen. Over the pure single phase the CuO and ZnO oxides methanol desorption occurred as broad TPD peaks centered slightly higher than 400 K. These were accompanied by very weak and broad desorption peaks for CH_2O that exhibited the same thermal behavior, as shown in Figs. 3 and 4. At higher temperature, TPSR also resulted in the appearance of H_2 and CO_2 over CuO and H_2 and CO (with small amounts of CO_2) over ZnO. Over the multicomponent catalysts, the temperatures of the TPSR peaks resembled those observed with CuO, rather than the high temperature behavior of ZnO. Over these catalysts, the CH_3OH, CH_2O, and H_2 desorption can be explained by the following reaction scheme (48):

$$CH_3OH(a) \rightleftarrows CH_3OH(g) \qquad [5]$$

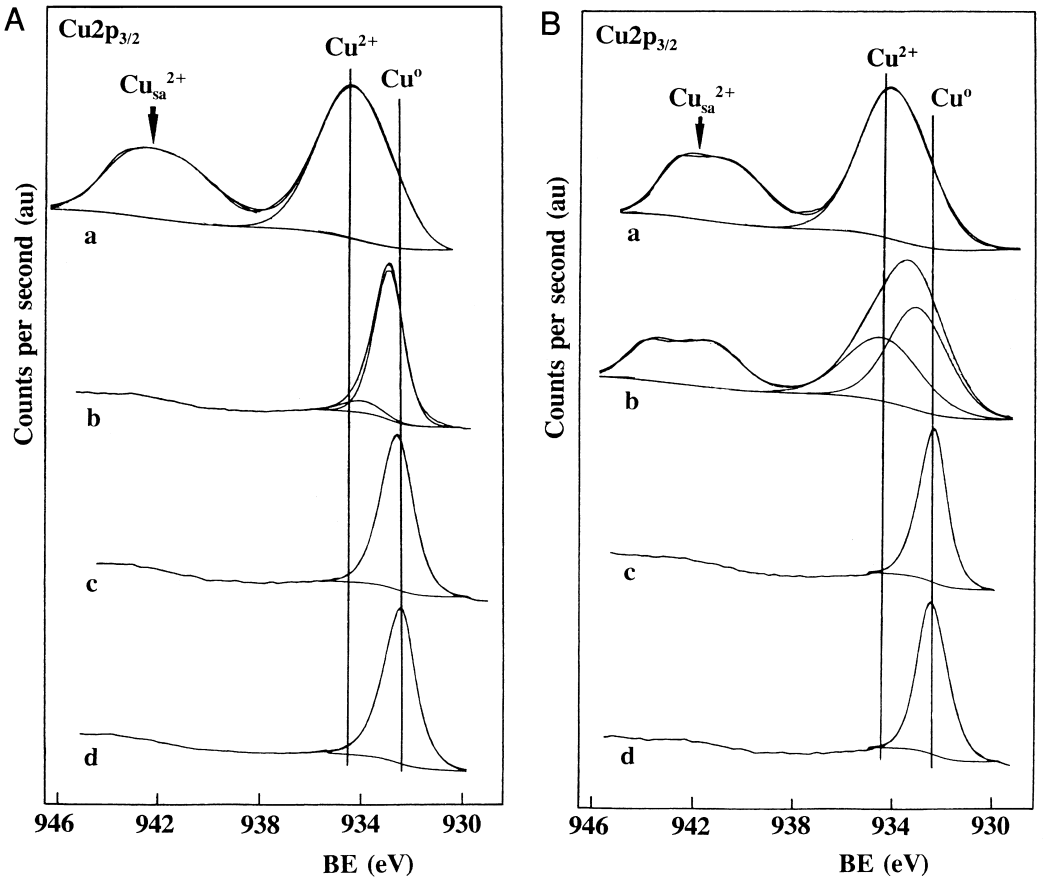

FIG. 2. (A) Cu $2p_{3/2}$ core level spectra of catalyst B calcined at 553 K and subjected to several pretreatments within the preparation chamber of the electron spectrometer: (a) outgassing at room temperature; (b) H_2-reduction at 473 K for 1 h; (c) H_2-reduction at 523 K for 1 h; and (d) H_2-reduction at 573 K for 1 h. (B) Cu $2p_{3/2}$ core level spectra of Cs-doped catalyst B subjected to several pretreatments: (a) outgassing at room temperature; (b) H_2-reduction at 473 K for 1 h; (c) H_2-reduction at 523 K for 1 h; (d) H_2-reduction at 473 K for 1 h.

$$CH_3OH(a) \rightleftarrows CH_3O(a) + H(a) \quad [6]$$

$$CH_3O(a) \rightleftarrows H_2CO(a) + H(a) \quad [7]$$

$$H_2CO(a) \rightleftarrows H_2CO(g) \quad [8]$$

$$H(a) + H(a) \rightleftarrows H_2(a) \quad [9]$$

$$H_2(a) \rightleftarrows H_2(g). \quad [10]$$

The relative quantities of desorbed methanol and formaldehyde depended on the catalyst promotion. Over copper oxide (Fig. 3), zinc oxide (Fig. 4), unpromoted catalyst A (Fig. 5), and unpromoted catalyst B (Fig. 6), formaldehyde/methanol ratios were lower than over the cesium-promoted catalyst A (Fig. 7) and B (Fig. 8). It seems that cesium modified the equilibrium of reactions [6] and/or [7], shifting to the right. At temperatures between 400 and 500 K, a simultaneous desorption of hydrogen and CO_2 was observed, which might well be attributed to formate surface species (49). The amount of H_2 and CO_2 desorbed relative to the methanol peak was also modified by cesium incorporation to the catalyst. Thus, the $CO_2(H_2)$/methanol ratio was higher for undoped catalyst A (Fig. 5) and B (Fig. 6) than for the cesium-promoted counterparts CsA (Fig. 7) and CsB (Fig. 8). Therefore, it appears that the formation of formate surface species from adsorbed methanol is inhibited by the presence of cesium. On zinc oxide (Fig. 4) a different mechanism seems to be operative. Note that a simultaneous desorption of hydrogen and carbon monoxide occurred at temperatures between 450 and 600 K, which may also arise from formate surface species (49).

Other minor desorption products, including dimethyl ether (DME) and acetaldehyde were also detected. DME was desorbed from the copper sample (Fig. 3), and from the unpromoted catalyst A (Fig. 5) and B (Fig. 6), in good agreement with their selectivity to DME in CO hydrogenation (see below), indicating surface acidity. The desorption peak of acetaldehyde was found to be of very low intensity, if any, in unpromoted catalysts, but more intense in the cesium-promoted counterparts. This finding can be taken as

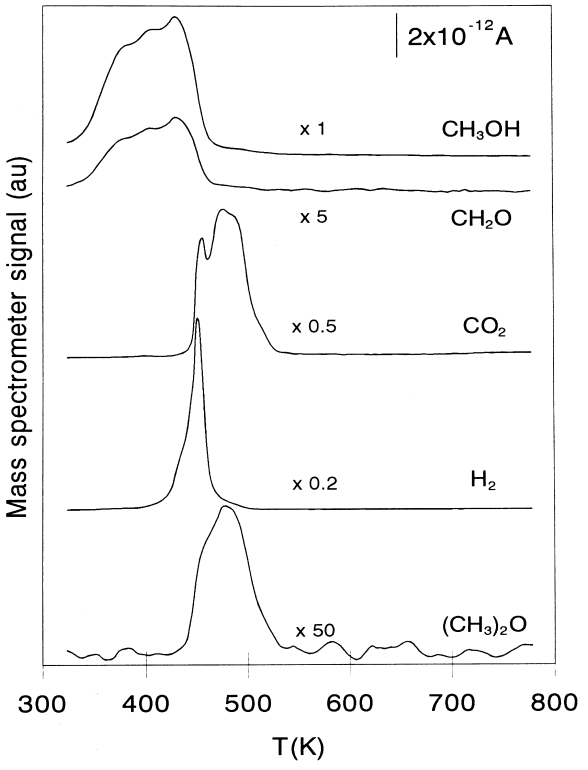

FIG. 3. Desorption flux of different species as a function of temperature after methanol adsorption at room temperature on reduced CuO. Magnification is given for each profile.

indicative of the formation of higher oxygenates by coupling of two C_1 surface species, such an effect being enhanced by the presence of cesium. It can be noted that, although acetaldehyde was not detected on copper (Fig. 3), it was clearly observed on zinc oxide (Fig. 4), but at higher temperatures than on promoted catalyst CsA (Fig. 7) and CsB (Fig. 8). Therefore, cesium promotion on Cu–Zn–Cr catalysts has a double effect: (i) elimination of surface acidity as revealed by suppression of DME formation (Figs. 7 and 8), and (ii) improving the carbon–carbon bond formation between surface species on basic centers, as detected by the desorption peak of acetaldehyde. Accordingly, this latter effect agrees with previous suggestions by Nunan *et al.* (5, 12). The C–C bond formation on zinc oxide at higher temperatures than on the cesium-promoted catalysts could be related to the lower basicity of zinc oxide than of cesium-promoted catalysts.

Catalytic Activity in CO Hydrogenation

Activity and selectivity results of CO hydrogenation with and without cofeeding methanol, ethanol, or 1-propanol are compiled in Tables 4–6. When the catalyst with high surface area was doped with cesium (catalyst CsB), an increase in the formation of methanol from CO/H_2 is observed (Table 4), as earlier reported by Nunan *et al.* (18). Furthermore, an increase in the formation of higher alcohols ($C_{2+}OH$) was noted, especially becoming larger for 1-propanol and isobutanol. In addition to this, larger quantities of esters and a decrease in ether formation (DME) are produced. As DME is formed on acid sites, its inhibition could be explained by the neutralization of surface acid sites by cesium incorporation. Ester formation over the cesium doped catalyst is in agreement with the previous TPSR observations showing the desorption of aldehyde compounds, wherein the esters may arise from the coupling reaction of aldehyde species with surface alkoxide species, very likely on surface sites involving cesium (10). When methanol was cofed, a small increase in the formation of $C_{2+}OH$ was observed. Instead, when the alcohol fed was ethanol, an appreciable increase in the yield of C_3 and C_4 alcohols was apparent. This observation provides an argument that adsorbed ethanol species could be intermediate in the synthesis of $C_{3+}OH$ alcohols. A similar effect on isobutanol formation was observed when 1-propanol was cofed. Consequently, from the selectivity toward higher alcohols obtained under the conditions of CO hydrogenation with alcohol cofeeding (Tables 4–6), it is evident that the most difficult step in higher alcohol synthesis is $C_1OH \rightarrow C_2OH$.

The comparison of activity data for catalysts A and B (Tables 4 and 5) shows that the catalyst calcined at lower temperature (catalyst B) is more active and more selective

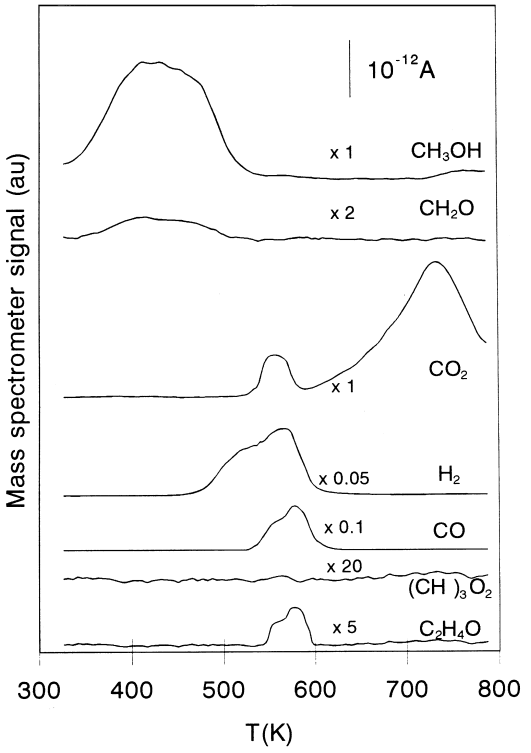

FIG. 4. Desorption flux of different species as a function of temperature after methanol adsorption at room temperature on reduced ZnO. Magnification is given for each profile.

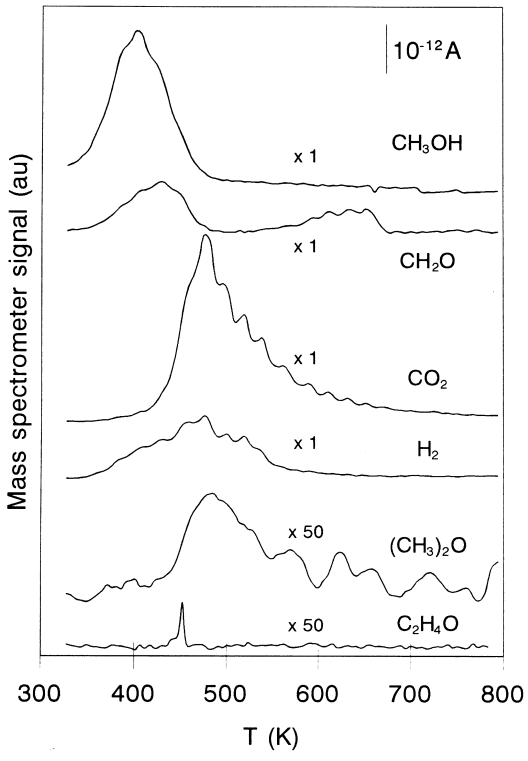

FIG. 5. Desorption flux of different species as a function of temperature after methanol adsorption at room temperature on reduced catalyst A. Magnification is given for each profile.

to higher alcohols. Bearing in mind that conversion levels are higher for catalysts with higher surface area (B and CsB) than for that calcined at higher temperature (A and CsA), the differences in selectivity can be attributed to changes in concentration of surface species. On the other hand, as recently reported, alcohol selectivities could be modified by catalyst porosity (50, 51). In line with this, a more porous catalyst produces more higher alcohols. As no ether formation was detected with catalysts A and CsA, the absence of surface acidity may be explained by the formation of zinc chromite spinel, as detected by XRD, during calcination at 673 K, which inhibits the acidity of chromium oxide. Accordingly, the effect of cesium doping on sample A is similar to that observed in sample B, confirming the role of Cs promoter in the reaction. Comparison of Tables 5 and 6 provides a basis for establishing the effect of reaction temperature on catalytic selectivity upon increasing the reaction temperature with $H_2/CO = 0.45$, a decrease in methanol production and an increase in selectivity toward higher alcohols selectivity was shown, in agreement with previous studies (5, 7). Also, hydrocarbon formation is observed at higher temperatures. It seems that the cesium promotion is more pronounced at lower reaction temperatures, i.e., 548 K. This effect can be explained by kinetic enhancement induced by Cs coupled with high conversion of the reactants and equilibria that become important at the higher reaction temperature.

CONCLUSION

The cesium promotion of the ternary Cu–Zn–Cr oxide catalyst has been investigated in the high pressure hydrogenation of CO to form alcohols. The structural investigation of the catalysts revealed that the reduction of copper was inhibited by incorporation of cesium. Under typical reaction conditions, both TPR and XPS revealed that detectable copper phases were completely reduced to metallic copper. The crystal sizes of copper particles tend to increasing with increasing reduction temperature, and this tends to be accompanied by simultaneous Cs segregation to the catalyst surface. The catalytic activity results from CO hydrogenation, with and without cofeeding methanol, ethanol, or 1-propanol, showing that a large surface area of the catalysts and ill-defined crystalline phases yields higher activity and a slight increase in HAS selectivity. However, cesium incorporation resulted in much higher methanol and $C_{2+}OH$ productivities. By cofeeding a given C_nOH alcohol, the $C_{n+1}OH$ yield was enhanced, thus suggesting that the most difficult chain growth steps is the reaction $2CH_3OH \rightarrow CH_3CH_2OH$.

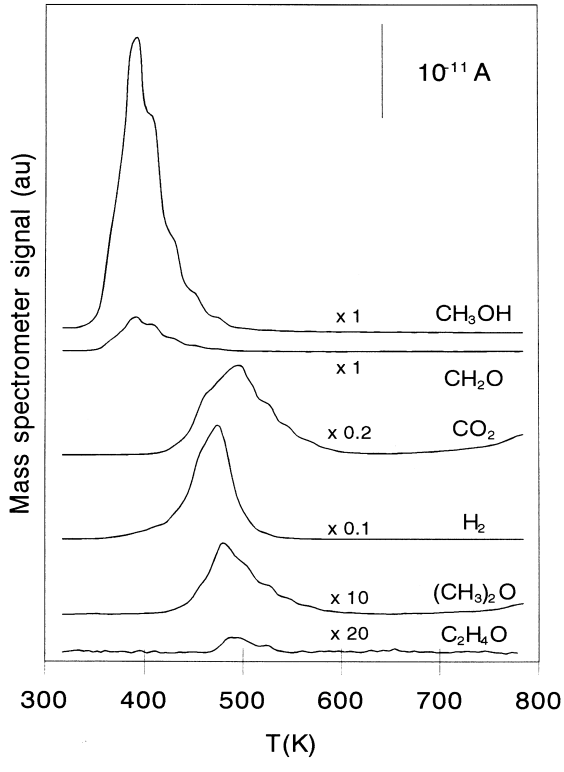

FIG. 6. Desorption flux of different species as a function of temperature after methanol adsorption at room temperature on reduced catalyst B. Magnification is given for each profile.

TABLE 4

Steady State Space Time Yields Obtained with $H_2/CO = 0.45$ Synthesis Gas and with Methanol (MeOH), Ethanol (EtOH), or 1-Propanol (1-PrOH) Injected into the Synthesis Gas; Reaction Conditions (P = 7.6 MPa, T = 548 K)

	Catalysts B				Catalysts CsB			
Y (g/kg_{cat} h)	CO/H_2	CO/H_2 + MeOH	CO/H_2 + EtOH	CO/H_2 + 1-PrOH	CO/H_2	CO/H_2 + MeOH	CO/H_2 + EtOH	CO/H_2 + 1-PrOH
CO_2	39.8	64.5	33.5	37.3	53.0	73.1	85.0	43.0
MeOH	200.0	*	85.6	76.9	270.9	*	97.0	77.0
EtOH	3.0	4.7	*	0.6	24.6	35.3	*	3.0
1-PrOH	—	—	17.7	*	13.3	14.8	22.8	*
IsoBuOH	—	—	17.3	19.8	13.7	18.2	23.1	40.3
Esters	—	1.0	6.1	—	8.7	10.8	19.0	2.7
Ethers	32.8	55.4	—	—	4.5	5.4	—	—

* Alcohol fed into the synthesis gas stream.

TABLE 5

Steady State Space Time Yields Obtained with $H_2/CO = 0.45$ Synthesis Gas and with Methanol (MeOH), Ethanol (EtOH), or 1-Propanol (1-PrOH) Injected into the Synthesis Gas; Reaction Conditions (P = 7.6 MPa, T = 548 K)

	Catalyst A				Catalyst CsA			
Y (g/kg_{cat} h)	CO/H_2	CO/H_2 + MeOH	CO/H_2 + EtOH	CO/H_2 + 1-PrOH	CO/H_2	CO/H_2 + MeOH	CO/H_2 + EtOH	CO/H_2 + 1-PrOH
CO_2	—	4.2	48.7	6.8	2.4	6.2	48.5	35.8
MeOH	8.8	*	10.7	5.2	84.2	*	40.7	43.2
EtOH	—	5.8	*	—	2.7	7.0	*	—
1-PrOH	—	—	6.0	*	—	0.4	16.7	*
IsoBuOH	—	—	—	8.1	—	—	13.9	16.6
Esters	—	—	40.0	—	—	—	—	—
Ethers	—	—	—	—	—	—	—	—

* Alcohol fed into the synthesis gas stream.

TABLE 6

Steady State Space Time Yields Obtained with $H_2/CO = 0.45$ Synthesis Gas and with Methanol (MeOH), Ethanol (EtOH) or 1-Propanol (1-ProOH) Injected into the Synthesis Gas; Reaction Conditions (P = 7.6 MPa, T = 583 K)

	Catalyst A				Catalyst CsA			
Y (g/kg_{cat} h)	CO/H_2	CO/H_2 + MeOH	CO/H_2 + EtOH	CO/H_2 + 1-PrOH	CO/H_2	CO/H_2 + MeOH	CO/H_2 + EtOH	CO/H_2 + 1-PrOH
CO_2	—	16.2	34.8	6.8	66.4	67.7	152.0	102.5
MeOH	8.2	*	8.5	5.2	73.8	*	65.5	60.7
EtOH	—	16.8	*	0	9.8	11.6	*	0.1
1-PrOH	—	0.4	39.9	*	10.5	15.9	32.9	*
IsoBuOH	—	—	5.5	8.1	2.1	2.1	13.8	20.9
Esters	—	—	—	—	—	—	31.9	—
Ethers	—	—	—	—	—	—	—	—

* Alcohol fed into the synthesis gas stream.

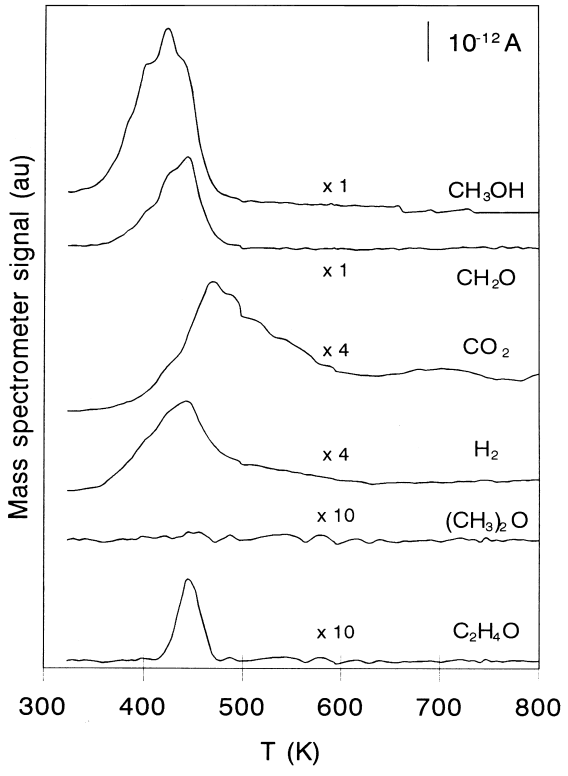

FIG. 7. Desorption flux of different species as a function of temperature after methanol adsorption at room temperature on reduced Cs-promoted catalyst CsA. Magnification is given for each profile.

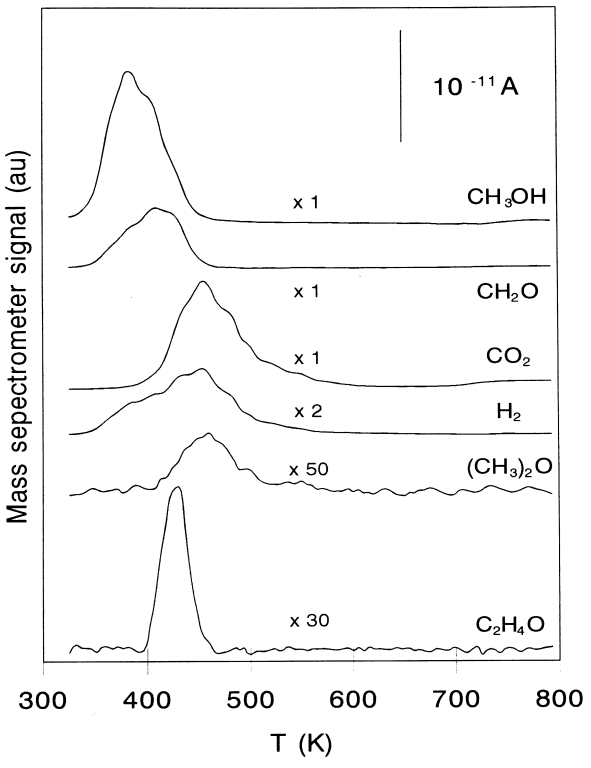

FIG. 8. Desorption flux of different species as a function of the desorption temperature after methanol adsorption at room temperature on reduced Cs-promoted catalyst CsB. Magnification is given for each profile.

ACKNOWLEDGMENTS

J. M. C. M. acknowledges a scholarship grant from the Ministerio de Educacion y Ciencia (Spain). The partial financial support of this work by the CICYT (Project No. MAT91-0494) and U.S. Department of Energy is also gratefully acknowledged.

REFERENCES

1. Morandi, F., Trotta, R., Precci, G., and Sposini, M., *Energy Prog.* **8**(1), 1 (1988).
2. Natta, G., Colombo, U., and Pasquon, I., *in* "Catalysis" (P. H. Emmett, Ed.), Vol. V, Chap. 3, Reinhold, New York, 1957.
3. Forzatti, P., Tronconi, E., and Pasquon, I., *Catal. Rev.-Sci. Eng.* **33**(1&2), 109 (1988).
4. Smith, K. J., and Anderson, R. B., *Canad. J. Chem. Eng.* **61**, 40 (1983).
5. Klier, K., Herman, R. G., and Young, C.-W., *Preprints, Div. Fuel Chem., ACS* **29**(5), 273 (1984).
6. Klier, K., *in* "Catalysis on the Energy Scene" (S. Kaliaguine and A. Mahay, Eds.), p. 439. Elsevier, Amsterdam, 1984.
7. Slaa, J. C., van Ommen, J. G., and Ross, J. R. M., *Catal. Today* **15**, 129 (1992).
8. Morgan, G. T., *Proc. R. Soc. London A* **127**, 246 (1930).
9. Morgan, G. T., Hardy, D. V. N., and Procter, R. H., *J. Soc. Chem. Ind.* **51**, 1T (1932).
10. Vedage, G. A., Himelfarb, P. B., Simmons, G. W., and Klier, K., *ACS Symp. Ser.* **279**, 295 (1985).
11. Calverley, E. M., and Anderson, R. B., *J. Catal.* **104**, 434 (1987).
12. Nunan, J. G., Bogdan, C. E., Klier, K., Smith, K. J., Young, C.-W., and Herman, R. G., *J. Catal.* **113**, 410 (1988).
13. Nunan, J. G., Bogdan, C. E., Klier, K., Smith, K. J., Young, C.-W., and Herman, R. G., *J. Catal.* **116**, 195 (1989).
14. Nunan, J. G., Herman, R. G., and Klier, K., *J. Catal.* **116**, 222 (1989).
15. Hofstadt, C. E., Kochloefl, K., and Bock, O., German Patent 3,005,551 (Aug. 20, 1981), assigned to Süd-Chemie AG.
16. Kihuzono, Y., Kagami, S., Naito, S., Onishi, T., and Tamaru, K., *J. Chem. Soc. Faraday Discuss.* **72**, 135 (1982).
17. Davies, P., and Snowdon, F. R., U.S. Patent 3,326,956 (June 20, 1967); Collins, B. M., U.S. Patent 3,850,850 (Nov. 26, 1974), assigned to Imperial Chemical Industries Ltd.; Stiles, A. B., U.S. Patent 4,111,847 (Sept. 5, 1978), assigned to E. I. DuPont de Nemours and Co.
18. Nunan, J. G., Klier, K., Young, C.-W., Himelfarb, P. B., and Herman, R. G., *J. Chem. Soc. Chem. Commun.* **193**, (1986).
19. Klier, K., Herman, R. G., and Vedage, G. A., U.S. Patent 4,843,101 (June 27, 1989), assigned to Lehigh University.
20. Kung, H. H., *Catal. Rev. Sci. Eng.* **22**, 235 (1980).
21. Klier, K., "Advances in Catalysis" (D. D. Eley, P. W. Selwood, and P. B. Weisz, Eds.), Vol. 31, p. 234. Academic Press, San Diego, 1982.
22. Klier, K., Herman, R. G., Nunan, J. G., Smith, K. J., Bogdan, C. E., Young, C.-W., and Santiesteban, J. G., *in* "Methane Conversion" (D. M. Bibby, C. D. Chang, R. F. Howe, and S. Yurchak, Eds.), p. 109. Elsevier, Amsterdam, 1988.
23. Klier, K., Herman, R. G., Himelferab, P. B., Young, C.-W., Hou, S., and Marcos, J. A., *in* "New Frontiers in Catalysis" (L. Guczi, F. Solymosi, and P. Tétényi, Eds.), Vol. 1442, Elsevier/Akadémiai Kiad, Budapest, 1993.
24. Edwards, J. F., and Schrader, G. L., *J. Phys. Chem.* **88**, 5620 (1984).
25. Edwards, J. F., and Schrader, G. L. *J. Catal.* **94**, 175 (1985).

26. Deluzarche, A., Kieffer, R., and Muth, A., *Thetraedrom Lett.* **38**, 3357 (1977).
27. Deluzarche, A., Hindermann, J. P., Kiennemann, A., and Kieffer, R., *J. Mol. Catal.* **31**, 225 (1985).
28. Vedage, G. A., Herman, R. G., and Klier, K., *J. Catal.* **95**, 423 (1985).
29. Vedage, G. A., Pitchai, R., Herman, R. G., and Klier, K., *in* "Proceedings, 8th International Congress on Catalysis, Berlin 1984," Vol. II, p. 47. Verlag-Chemie, Weinheim, 1984.
30. Fu, S. S., and Somorjai, G. A., *J. Phys. Chem.* **96**, 4542 (1992).
31. Waugh, K. C., *Catal. Today* **15**, 51 (1992).
32. Waugh, K. C., *Catal. Today* **18**, 147 (1993).
33. Zhang, R., Ludviksson, A., and Campbell, C. T., *Catal. Lett.* **25**, 277 (1994).
34. Kagami, S., Naito, S., Kikuzono, Y., and Tamaru, K., *J. Chem. Soc. Chem. Commun.* **256**, (1983).
35. Hinderman, J. P., Hutchings, G. J., and Kiennemann, A., *Catal. Rev.-Sci. Eng.* **35**(1), 1 (1993).
36. Mazanec, T. J., *J. Catal.* **98**, 115 (1986).
37. Herman, R. G., Bogdam, C. E., Klumer, P. L., and Nuszkowski, D. M., *Mat. Chem. Phys.* **35**, 233 (1993).
38. Shiskov, D. S., Strovrakova, D. A., and Kasabona, N. A., *Kinet. Kataliz.* **21**, 1559 (1980).
39. Guerrero-Ruiz, A., Rodriguez-Ramos, I., and Fierro, J. L. G., *Appl. Catal.* **72**, 119 (1991).
40. Gorriz, O., Cortes, V., and Fierro, J. L. G., *Ind. Eng. Chem. Res.* **31**, 2670 (1992).
41. Kim, K. S., *J. Electron. Spectrosc. Rel. Phenom.* **3**, 217 (1974).
42. Fleisch, T. H., and Mains, G. J., *Appl. Surf. Sci.* **10**, 51 (1982).
43. Tobin, J. P., Hirschwald, W., and Cunningham, J., *Appl. Surf. Sci.* **16**, 441 (1983).
44. Sepulveda, A., Marquez, C., Rodriguez-Ramos, I., Guerrero-Ruiz, A., and Fierro, J. L. G., *Surf. Interface Anal.* **20**, 1067 (1993).
45. Scheffer, G. R., and King, T. S., *J. Catal.* **116**, 488 (1989).
46. Moretti, G., and Porta, P., *Surf. Interface Anal.* **15**, 47 (1990).
47. Garentrom, J. W., and Winograd, N., *J. Chem. Phys.* **67**, 3500 (1977).
48. Bowker, M., and Madix, R. J., *Surf. Sci.* **95**, 190 (1980).
49. Bowker, M., Houghton, H., and Waugh, K. C., *J. Catal.* **84**, 252 (1983).
50. Brendt, H., Briehen, V., Evert, S., Gutschick, D., and Kotowski, W., *Catal. Lett.* **14**, 185 (1992).
51. Campos-Martín, J. M., Guerrero-Ruiz, A., and Fierro, J. L. G., *J. Catal.* **156**, 208 (1995).